

Phonon Dispersion Relations in $\text{PrBa}_2\text{Cu}_3\text{O}_{6+x}$ ($x \approx 0.2$)

C. H. Gardiner,^{1,*} A. T. Boothroyd,² B. H. Larsen,³ W. Reichardt,⁴
A. A. Zhokhov,⁵ N. H. Andersen,⁶ S. J. S. Lister,⁷ and A. R. Wildes⁸

¹*National Physical Laboratory, Queens Road, Teddington, Middlesex, TW11 0LW, UK*

²*Clarendon Laboratory, University of Oxford, Parks Road, Oxford, OX1 3PU, UK*

³*NKT Research and Innovation, Blokken 84, 3460 Birkerød, Denmark*

⁴*Forschungszentrum Karlsruhe, IFP, Postfach 3640, D-76021 Karlsruhe, Germany*

⁵*Russian Academy of Sciences, Institute of Solid State Physics, Chernogolovka 14232, Russia*

⁶*Risø National Laboratory, Frederiksborgvej 399, P.O. 49, DK-4000 Roskilde, Denmark*

⁷*Oxford Magnet Technology Ltd, Wharf Road, Eynsham, Witney, Oxfordshire, OX29 4BP, UK*

⁸*Institut Laue-Langevin, Boîte Postale 156, F-38042, Grenoble Cédex 9, France*

(Dated: March 22, 2022)

We report measurements of the phonon dispersion relations in non-superconducting, oxygen-deficient $\text{PrBa}_2\text{Cu}_3\text{O}_{6+x}$ ($x \approx 0.2$) by inelastic neutron scattering. The data are compared with a model of the lattice dynamics based on a common interatomic potential. Good agreement is achieved for all but two phonon branches, which are significantly softer than predicted. These modes are found to arise predominantly from motion of the oxygen ions in the CuO_2 planes. Analogous modes in $\text{YBa}_2\text{Cu}_3\text{O}_6$ are well described by the common interatomic potential model.

PACS numbers: 74.72.-h, 63.20.Dj, 61.12.Ex

I. INTRODUCTION

The suppression of superconductivity by praseodymium in $\text{PrBa}_2\text{Cu}_3\text{O}_{6+x}$ has for some years presented an outstanding problem in the field of cuprate superconductivity.^{1,2} Although superconductivity at $T_c \approx 90\text{K}$ is exhibited by the majority of compounds with the composition $R\text{Ba}_2\text{Cu}_3\text{O}_7$, where R is a rare-earth, $\text{PrBa}_2\text{Cu}_3\text{O}_{6+x}$ combines antiferromagnetic ordering with semiconducting resistivity across the whole of the known phase diagram ($0 < x < 1$).

An influential model of the electronic structure of $\text{PrBa}_2\text{Cu}_3\text{O}_{6+x}$ ³ suggests that the absence of superconductivity is caused by localisation of holes due to hybridisation of the Pr $4f$ and O $2p$ orbitals. This is supported by the observation of an enhanced ordering temperature T_{Pr} of the Pr sublattice, which is an order of magnitude larger than the ordering temperature T_R of the rare-earth sublattice in other $R\text{Ba}_2\text{Cu}_3\text{O}_7$ compounds.

Neutron scattering studies of the magnetic structure⁴ and dispersive magnetic excitations^{5,6} have probed the strengths of the different magnetic couplings in $\text{PrBa}_2\text{Cu}_3\text{O}_{6+x}$, and indicate that the high value of T_{Pr} is partly due to an enhanced Pr–O–Pr superexchange and partly due to the presence of a significant coupling between the Cu and Pr sublattices. Both of these effects could be the result of hybridisation between Pr $4f$ electrons and the CuO_2 planes.

Hybridisation is expected to affect the phonon dispersion relations through the Pr–O bonds. In this paper we present measurements of the phonon dispersion relations, performed by inelastic neutron scattering on an oxygen-deficient single crystal of $\text{PrBa}_2\text{Cu}_3\text{O}_{6+x}$ ($x \approx 0.2$). The data are compared with a model of the lattice dynamics based on a common interatomic potential, which was originally developed for $\text{YBa}_2\text{Cu}_3\text{O}_6$ and later modified

for $\text{PrBa}_2\text{Cu}_3\text{O}_6$.⁷

II. EXPERIMENTAL DETAILS

The single crystal sample of $\text{PrBa}_2\text{Cu}_3\text{O}_{6+x}$ was prepared by top seeding a flux and had a mass of $\sim 2\text{g}$. It was reduced at 700°C in a flow of 99.998% argon for 100 hours and quenched to room temperature resulting in an estimated oxygen content of $x \approx 0.2$. Using x-ray Laue diffraction it was aligned with the $[1\bar{1}0]$ direction vertical. It was then glued onto an aluminium mount using G.E. varnish and held securely in place with aluminium wire. Preliminary neutron diffraction measurements showed the crystal mosaic to be $\sim 1^\circ$.

The neutron scattering experiments were performed on the IN1 and IN22 triple-axis spectrometers at the Institut Laue-Langevin research reactor. The configuration of IN1 was as follows: flat copper (200) monochromator, pyrolytic graphite (002) analyser with horizontal and slight vertical focussing, no collimation before the monochromator, $60'$ collimator between the monochromator and sample, and pyrolytic graphite filter between the sample and analyser to reduce contamination of the beam by second and higher order reflections from the monochromator. The spectrometer was operated in the constant k_f configuration with a final energy of 34.8meV . Low efficiency beam monitors, placed before the monochromator and between the filter and the analyser, were used to gauge the incident beam intensity and to check for accidental Bragg scattering. The crystal was mounted inside a displax refrigerator and aligned such that the $[110]$ and $[001]$ directions lay within the scattering plane. All measurements were performed at $T = 12\text{K}$. The configuration of IN22 was identical except for the use of a vertically curved pyrolytic graphite (002) monochroma-

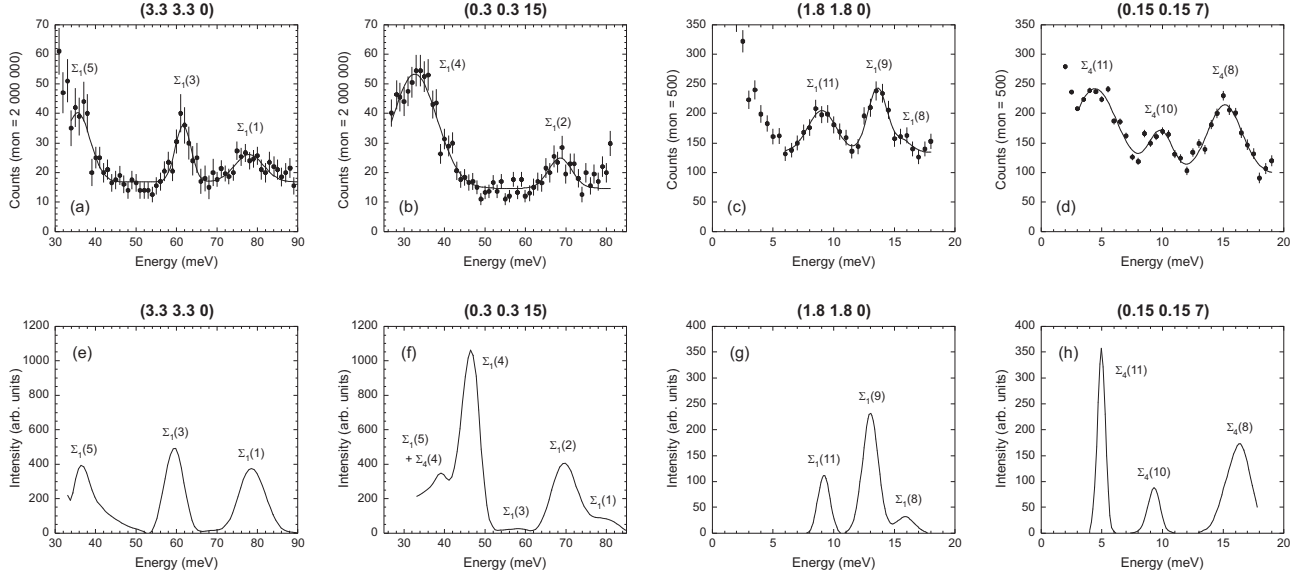


FIG. 1: Plots (a), (b), (c) and (d) show typical energy scans. The points are the raw neutron scattering data (averaged over several runs with different, overlapping energy ranges), and the lines are Gaussian fits. The value of \mathbf{Q} is shown at the top of each plot. In plots (a) and (b), from IN1, a monitor count of 2×10^6 corresponds to a counting time of 2–5 minutes per point (depending on energy), while in plots (c) and (d), from IN22, a monitor count of 500 corresponds to ~ 2 minutes per point. Plots (e), (f), (g) and (h) show simulations of the energy-scans, produced from the common interatomic potential model described in the text, which facilitate the assignment of symmetry labels to the different phonon branches.

tor, no collimators and a fixed final energy of 14.7 meV. A low efficiency beam monitor placed before the monochromator was used to gauge the incident beam intensity, but there was no monitor between the filter and the analyser to check for accidental Bragg scattering. The crystal was mounted inside a helium cryostat and aligned such that the [110] and [001] directions lay within the scattering plane. Most of the measurements were performed at a temperature of 1.6 K.

III. MEASUREMENTS

The phonon dispersion relations in $\text{PrBa}_2\text{Cu}_3\text{O}_{6.2}$ were measured by performing a series of constant \mathbf{Q} energy scans at positions across the Brillouin zone (\mathbf{Q} is the neutron scattering vector). On IN1, scans were performed over an energy range $\hbar\omega = 30\text{--}90\text{ meV}$ with $\mathbf{Q} = (3 \pm h, 3 \pm h, 0)$ to excite predominantly longitudinal modes and $\mathbf{Q} = (h, h, 15)$ to excite predominantly transverse modes. On IN22, scans were performed over an energy range $\hbar\omega = 0\text{--}24\text{ meV}$ with $\mathbf{Q} = (2 - h, 2 - h, 0)$, $(0, 0, 7 + l)$ to excite predominantly longitudinal modes and $\mathbf{Q} = (h, h, 7)$, $(h, h, 8)$, $(2, 2, l)$ to excite predominantly transverse modes. Large values of \mathbf{Q} were chosen to maximise the phonon scattering cross section (which is proportional to Q^2), while minimising the cross section for magnetic crystal field excitations (which scales with the magnetic form factor, falling off at high Q).⁸

The scattering intensity of a phonon mode is determined by its dynamical structure factor, a quantity that varies within each Brillouin zone and also between different zones. This means that some modes have a measurable intensity only at certain points within each Brillouin zone. In such cases, or when a scan was contaminated by accidental Bragg scattering, energy scans were performed in neighbouring ($\pm h$) Brillouin zones to gain as many points on the dispersion curves as possible.

Some typical scans taken on IN1 and IN22 are shown in Figs. 1 (a)–(d). The peaks are quite broad because of the horizontal focussing of the analysers. There is little evidence of magnetic scattering due to crystal field excitations, which are known to exist in $\text{PrBa}_2\text{Cu}_3\text{O}_6$ at energies of 61.5, 65.2, 76.0 and 84.7 meV,⁹ but it is possible that a small amount of magnetic scattering might contribute to the broadness of the observed phonon branches in the energy range 70–90 meV.

To determine the dispersion of the observed phonon modes in an unbiased way, each energy scan was fitted with a lineshape constructed from several gaussians superimposed on a constant background. The centres, amplitudes and linewidths of the gaussians and the height of the background were refined using a least squares method. Figure 2 shows the dispersion curves obtained by plotting the peak centres as a function of the phonon wavevector \mathbf{q} , where \mathbf{q} is obtained from

$$\mathbf{Q} = \mathbf{q} + \boldsymbol{\tau}, \quad (1)$$

and τ is a reciprocal lattice vector.

IV. MODEL

A model based on a common interatomic potential was previously developed for the phonon dispersion curves in $\text{YBa}_2\text{Cu}_3\text{O}_6$.⁷ We adapted this for $\text{PrBa}_2\text{Cu}_3\text{O}_6$ by inserting the appropriate lattice parameters, atomic masses and nuclear scattering lengths, and the model was used to calculate the frequencies and dynamical structure factors of the phonon modes at the points in reciprocal space where our measurements were performed.

Comparison of the \mathbf{Q} -variation of the predicted and observed modes allowed us to identify the symmetries of the different branches. In this process the predicted frequencies were used only as a guide. More weight was given to the correspondence between the predicted and observed intensities of the modes. To facilitate the comparison, simulations of the energy-scans were produced by combining the predicted dynamical structure factors with the spectrometer resolution function, calculated using the approximate Cooper-Nathans method.¹⁰

Figs. 1 (e)–(h) show the simulations corresponding to the selected raw data shown in plots (a)–(d). Most of the observed modes were in good qualitative agreement with the simulations, so assignment of the symmetries was clear. However, plots (b) and (f) show a clear discrepancy between the observed and predicted phonon spectra. We have assigned the large peak observed at 33 meV to the $\Sigma_1(4)$ mode (for clarity we have numbered the branches from highest to lowest in frequency). Although the energy of this peak corresponds better to the energies of the predicted $\Sigma_4(4)$ and $\Sigma_1(5)$ modes, its intensity corresponds much better to that of the $\Sigma_1(4)$ mode, so we are confident that our assignment is correct.

In Fig. 2 the measured dispersion curves are compared with those predicted by the model. The agreement is good for the majority of the observed branches. However, the model overestimates the energy of branch $\Sigma_1(1)$ by ~ 8 meV (2 THz) at the zone centre and the energy of branch $\Sigma_1(4)$ by ~ 10 meV (2.5 THz) over the whole of the Brillouin zone. The relative motions of the atoms in these branches are shown in Fig. 3, and it is clear that the motion of the copper and oxygen atoms in the CuO_2 planes dominates. Both branches change character somewhat between the centre and the edge of the Brillouin zone, so the diagrams indicate the motions of the atoms at both of these positions in reciprocal space.

The broad resolution function of the spectrometer caused some ambiguity in the assignment of mode symmetries at zone centre. This was due to the possibility that we could have accidentally detected out-of-plane modes propagating in transverse directions. For instance, when we attempted to measure phonons propagating along $[\text{hh}0]$ it is possible that we could also have picked up modes propagating along $[00\text{h}]$. This effect is only important at zone centre, so although it could partially account for the lowering of the $\Sigma_1(1)$ mode at zone centre, we are confident that it could not have caused us to wrongly assign the symmetry of the $\Sigma_1(4)$ mode.

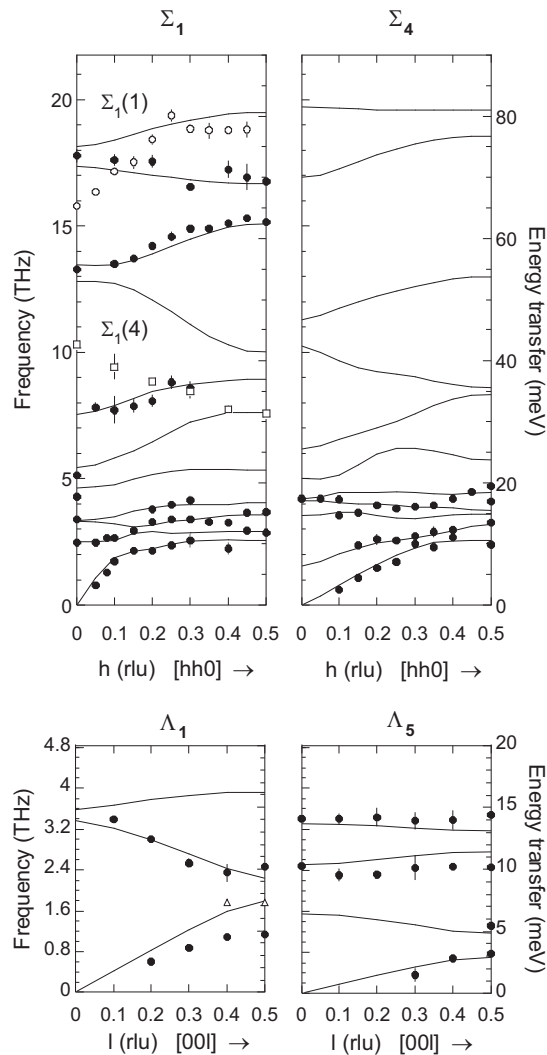


FIG. 2: Phonon dispersion curves in $\text{PrBa}_2\text{Cu}_3\text{O}_{6.2}$. The points are the fitted peak centres obtained from the constant \mathbf{Q} energy scans. The lines are the dispersion curves predicted by the common interatomic potential model, adapted from $\text{YBa}_2\text{Cu}_3\text{O}_6$ to $\text{PrBa}_2\text{Cu}_3\text{O}_6$. The x -axis is labelled with the h or l value of \mathbf{q} , where $\mathbf{q} = (hh0)$ or $(00l)$, in reciprocal lattice units (rlu). The Σ_1 modes were measured at $\mathbf{Q} = (3\pm h, 3\pm h, 0)$, $(h, h, 15)$ and $(2-h, 2-h, 0)$. The Σ_4 modes were measured at $\mathbf{Q} = (h, h, 7)$ and $(h, h, 8)$. The Λ_1 and Λ_5 modes were measured at $\mathbf{Q} = (0, 0, 7+l)$ and $(2, 2, l)$ respectively. Branches $\Sigma_1(1)$ and $\Sigma_1(4)$ are plotted as open circles and squares respectively. Both are significantly shifted with respect to the predictions of the model. The open triangles in the Λ_1 plot indicate modes that could not be indexed by comparison with the model. On IN22 there was no monitor to check for accidental Bragg scattering, so it is possible that this was the cause of these peaks.

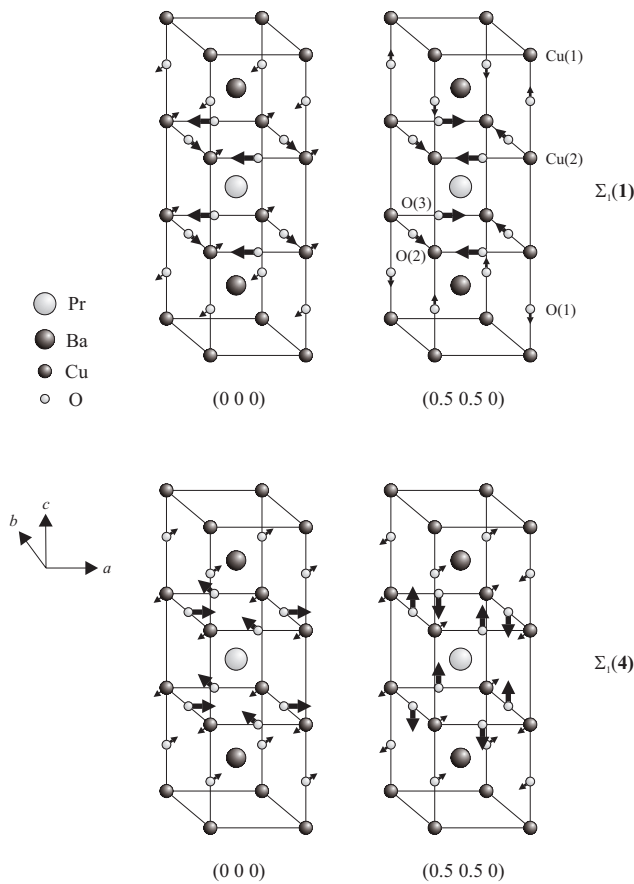


FIG. 3: Anomalous phonon modes. Branches $\Sigma_1(1)$ and $\Sigma_1(4)$ are shown at the Brillouin zone centre (0 0 0) and edge (0.5 0.5 0). The length and thickness of the arrows are approximately proportional to the magnitudes of the displacements obtained from the common interatomic potential model for $\text{PrBa}_2\text{Cu}_3\text{O}_{6+x}$ ($x = 0$). The measured compound ($x \approx 0.2$) has a partial occupancy of the two oxygen sites halfway between the Cu sites in the basal plane.

We now compare the dispersion curves we have observed in $\text{PrBa}_2\text{Cu}_3\text{O}_{6.2}$ with those previously observed in $\text{YBa}_2\text{Cu}_3\text{O}_6$.⁷ In $\text{YBa}_2\text{Cu}_3\text{O}_6$ all the branches are well described by the common interatomic potential model. Therefore the energy shifts of the $\Sigma_1(1)$ and $\Sigma_1(4)$ branches in $\text{PrBa}_2\text{Cu}_3\text{O}_{6.2}$ are anomalous. Although the $\Sigma_1(1)$ branch in $\text{YBa}_2\text{Cu}_3\text{O}_6$ has a similar shape to that

in $\text{PrBa}_2\text{Cu}_3\text{O}_{6.2}$ the dip at zone centre is not so pronounced. In contrast to $\text{PrBa}_2\text{Cu}_3\text{O}_{6.2}$, the $\Sigma_1(4)$ branch in $\text{YBa}_2\text{Cu}_3\text{O}_6$ fits well with the model. Although the energies of the other modes are very similar in both compounds, the $\Sigma_1(4)$ mode is ~ 12 meV (3 THz) higher in $\text{YBa}_2\text{Cu}_3\text{O}_6$ than in $\text{PrBa}_2\text{Cu}_3\text{O}_{6.2}$ throughout the Brillouin zone.

The common interatomic potential model assumes that the binding mechanism is predominantly ionic, but the anomalies we have observed suggest the existence of more complex binding mechanisms. It is particularly noteworthy that the anomalous phonon branches are characterised by large displacements of the oxygen atoms whose $2p$ orbitals are proposed to hybridise with the Pr $4f$ orbitals. Pr–O hybridisation, in which the Pr–O bonds are partially covalent in character, would result in a modified electron distribution around the in-plane O atoms, which could change the strength of the Cu–O bonds and alter certain vibrational modes.

V. CONCLUSION

We have described inelastic neutron scattering measurements of the phonon dispersion curves in oxygen-deficient single crystal $\text{PrBa}_2\text{Cu}_3\text{O}_{6+x}$ ($x \approx 0.2$). The results have been compared with a model of the lattice dynamics based on a common interatomic potential, which is found to overestimate the frequencies of two branches by a considerable amount. Strikingly, these branches are dominated by motion of the oxygen atoms in the CuO_2 planes: the same atoms that have been proposed to hybridise with the Pr orbitals. In contrast, the observed frequencies of all phonon branches in $\text{YBa}_2\text{Cu}_3\text{O}_6$ agree well with the model. The frequency shifts observed in the two anomalous branches in $\text{PrBa}_2\text{Cu}_3\text{O}_{6.2}$ are interpreted as indirect evidence for hybridisation of the Pr $4f$ and O $2p$ orbitals.

Acknowledgments

We would like to thank L.-P. Regnault and A. Ivanov for help with the experiments on IN22 and IN1 respectively. Financial support for C.H.G. by the EPSRC is also acknowledged.

* Electronic address before May 1, 2004: carol.gardiner@npl.co.uk; Electronic address after May 1, 2004: carol.webster@npl.co.uk

¹ H. B. Radousky, J. Mater. Res. **7**, 1917 (1992).

² A. T. Boothroyd, J. Alloys Compd. **303–304**, 489 (2000).

³ R. Fehrenbacher and T. M. Rice, Phys. Rev. Lett. **70**, 3471 (1993).

⁴ S. J. S. Lister, A. T. Boothroyd, N. H. Andersen, B. H.

Larsen, A. A. Zhokhov, A. N. Christensen, and A. R. Wildes, Phys. Rev. Lett. **86**, 5994 (2001).

⁵ A. T. Boothroyd, A. Longmore, N. H. Andersen, E. Brecht, and T. Wolf, Phys. Rev. Lett. **78**, 130 (1997).

⁶ C. H. Gardiner, S. J. S. Lister, A. T. Boothroyd, N. H. Andersen, A. A. Zhokhov, A. Stunault, and A. Hiess, Appl. Phys. A **74**, S898 (2002).

⁷ S. L. Chaplot, W. Reichardt, L. Pintschovius, and N. Pyka,

- Phys. Rev. B **52**, 7230 (1995).
- ⁸ G. L. Squires, *Introduction to the Theory of Thermal Neutron Scattering* (Dover Publications, Inc., Mineola, New York, USA, 1996).
- ⁹ G. Hilscher, E. Holland-Moritz, T. Holubar, H.-D. Jostarndt, V. Nekvasil, G. Schaudy, U. Walter, and G. Fillion, Phys. Rev. B **49**, 535 (1994).
- ¹⁰ M. J. Cooper and R. Nathans, Acta. Cryst. **23**, 357 (1967).